JPCBFK

FEBRUARY 17, 2011
VOLUME 115
NUMBER 6

pubs.acs.org/JPCB

THE JOURNAL OF PHYSICAL CHEMISTRY B

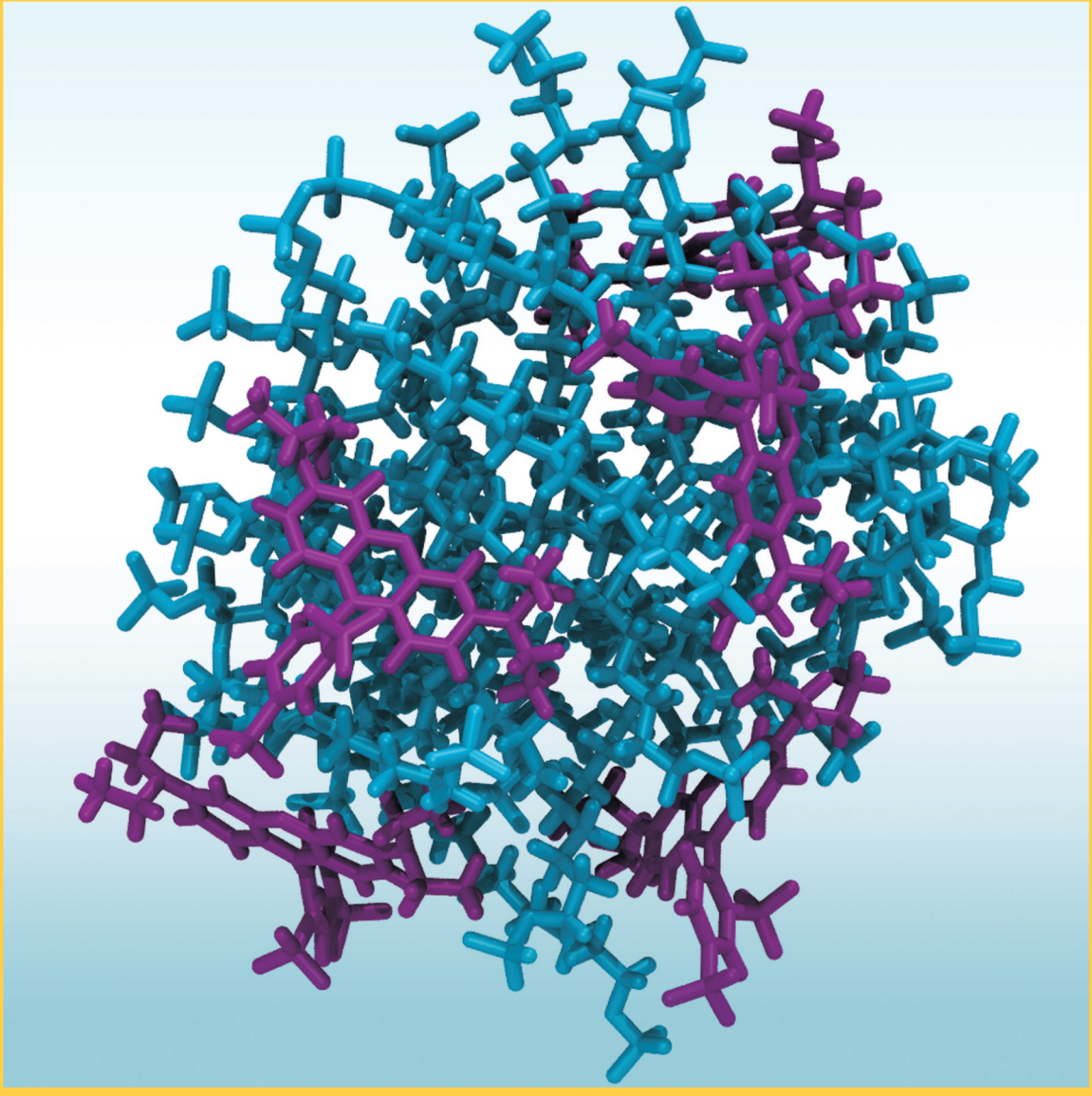

Molecular Dynamics Simulation Snapshot of Sulforhodamine B Incorporated into a Sodium Dodecyl Sulfate Micelle (see page 5A)

SOFT CONDENSED MATTER AND BIOPHYSICAL CHEMISTRY

ACS Publications
MOST TRUSTED. MOST CITED. MOST READ.

www.acs.org

THE JOURNAL OF PHYSICAL CHEMISTRY B

ARTICLE

pubs.acs.org/JPCB

Experimental and Molecular Dynamics Investigation into the Amphiphilic Nature of Sulforhodamine B

Baris E. Polat,[‡] Shangchao Lin,[‡,§] Jonathan D. Mendenhall,[‡] Brett VanVeller,[⊥] Robert Langer,[‡] and Daniel Blankschtein*[,‡]

[‡]Department of Chemical Engineering, [§]Department of Mechanical Engineering, and [⊥]Department of Chemistry, Massachusetts Institute of Technology, Cambridge, Massachusetts 02139, United States

ABSTRACT: Sulforhodamine B (SRB), a common fluorescent dye, is often considered to be a purely hydrophilic molecule, having no impact on bulk or interfacial properties of aqueous solutions. This assumption is due to the high water solubility of SRB relative to most fluorescent probes. However, in the present study, we demonstrate that SRB is in fact an amphiphile, with the ability to adsorb at an air/water interface and to incorporate into sodium dodecyl sulfate (SDS) micelles. In fact, SRB reduces the surface tension of water by up to 23 mN/m, and the addition of SRB to an aqueous SDS solution induces a significant decrease in the cmc of SDS. Molecular dynamics simulations were conducted to gain a deeper understanding of these findings. The simulations revealed that SRB has defined polar "head" and nonpolar "tail" regions when adsorbed at the air/water interface as a monomer. In contrast, when incorporated into SDS micelles, only the sulfonate groups were found to be highly hydrated, suggesting that the majority of the SRB molecule penetrates into the micelle. To illustrate the implications of the amphiphilic nature of SRB, an interesting case study involving the effect of SRB on ultrasound-mediated transdermal drug delivery is presented.

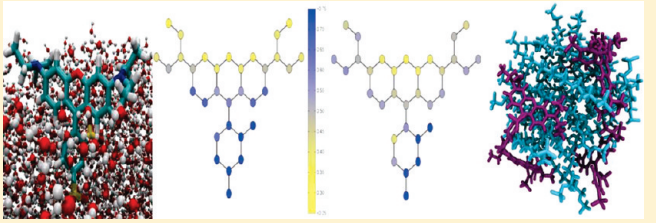

INTRODUCTION

Rhodamine dyes are a class of xanthene-derived molecules that are commonly used as laser dyes and fluorescent probes. Although most rhodamine dyes are cationic or have a net neutral charge (zwitterionic), there are forms of these dyes that have been imparted added water solubility, and a net negative charge, by aromatic sulfonation of the phenyl pendant group. One such molecule, sulforhodamine B (SRB; see Figure 1), has been used extensively during the past few decades as (i) a fluid-phase tracer,[1−3] (ii) a principal component in an assay for cytotoxicity,[4,5] and (iii) a model hydrophilic probe,[6−19] among others.

In spite of the widespread use of SRB, investigations into its chemical nature, especially with respect to its surface activity and interactions with surfactants, have been limited in scope in comparison to research done on other dyes, including several other rhodamines. For example, dyes such as rhodamine B[20−24] and rhodamine 6G[22,25−27] have been studied extensively with regard to (i) their adsorption at oil/water or air/water interfaces, (ii) their aggregation in aqueous solution as either dimers or higher-order aggregates, and (iii) their interactions with surfactant monomers and micelles. Many other fluorescent dyes, such as rose bengal[28,29] and various porphyrins,[30,31] have also been studied with regard to their interactions with surfactants and their solubilization within, or association with, micelles. This is because dye−surfactant interactions can lead to the breakup of dye dimers or to the solubilization of dyes in the palisade layer or nonpolar core of micelles, both of which can have dramatic consequences on the dye absorption and fluorescence wavelength and intensity.[32,33] For example, an amplification of fluorescence has even been observed for certain fluorophores when they associate with surfactants.[34−36]

Like many dyes, SRB is known to dimerize in solution,[20] and it belongs to a family of dyes that have been shown to include amphiphiles (such as the aforementioned rhodamine B[24] and rhodamine 6G[25]). However, in contrast to other rhodamine dyes, SRB adsorption has only been studied with respect to charged surfaces (such as cationic octadecylamine Langmuir−Blodgett films and anionic silica glass[37−39]), with minimal investigation into its activity at polar/nonpolar interfaces or its potential interaction with surfactants in aqueous solutions. The likely reason for this lack of investigation is due to the relatively high water solubility of SRB compared to other rhodamine dyes, which has led some to designate SRB as a "model hydrophilic" fluorescent probe.[6−19] However, as will be demonstrated experimentally in this paper, SRB does not behave as a simple salt, and it has the ability to (i) adsorb at an air/water interface, causing a decrease in surface tension, and (ii) interact strongly with surfactants in aqueous media, inducing significant changes in the driving force for micellization, as evidenced by a significant decrease in the critical micelle concentration (cmc) of sodium dodecyl sulfate (SDS) upon mixing with SRB.

Received: October 14, 2010
Revised: December 8, 2010
Published: January 11, 2011

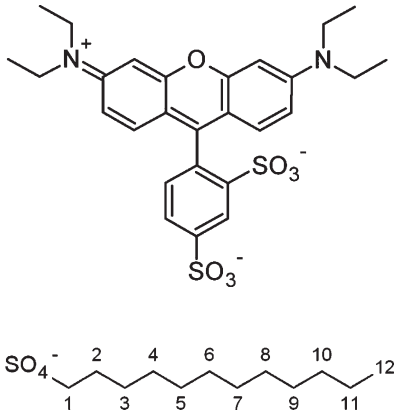

Figure 1. Chemical structures of sulforhodamine B (top) and sodium dodecyl sulfate (bottom), where the sodium counterion corresponding to both molecules is not shown for clarity.

In the present study, the amphiphilic nature of SRB is investigated both experimentally and using molecular dynamics simulations. Experimentally, surface tension measurements are used to study SRB adsorption at air/water interfaces, including its ability to affect the cmc of the commonly used anionic surfactant, SDS. The extent of SRB incorporation into SDS micelles is also investigated experimentally. To elucidate the experimental findings, bulk and interfacial molecular dynamics (MD) simulations of SRB in aqueous solution were conducted, both in the absence and in the presence of SDS. Such simulations provide a useful means for elucidating dye−surfactant interactions and may be applied more broadly to other dyes, thus minimizing the need for rigorous spectroscopic experimental measurements.

Finally, to illustrate the implications of the amphiphilic nature of SRB, an interesting case study on the effect of SRB on transdermal drug delivery using low-frequency ultrasound is presented. Amphiphilic molecules are known to act synergistically with low-frequency ultrasound in inducing skin permeability enhancement, which motivated the case study to further test the amphiphilicity of SRB.[40,41] The results obtained with SRB are compared to those obtained with the nonamphiphilic dye allura red (red food coloring).

EXPERIMENTAL SECTION

Materials. Sulforhodamine B (SRB), sodium dodecyl sulfate (SDS), and phosphate buffered saline (PBS) were obtained from Sigma-Aldrich Co. (St. Louis, MO). Allura red was obtained from TCI America (Portland, OR). All chemicals were used as received. Milli-Q (Millipore Corp., Billerica, MA) water was used for the preparation of all aqueous solutions.

Surface Tension Measurements. The surface tensions of aqueous solutions of SDS, SRB, and SDS in 9 mM SRB were measured as a function of concentration using a Krüss K11 tensiometer (Hamburg, Germany). The plate method was utilized with a titanium Wilhelmy plate (Krüss, wetting length of 42 mm). For each measurement, 20 surface tension readings were obtained, 3 s apart, and the final 10 readings were averaged to yield the surface tension for that measurement (with the first 10 measurements serving as an equilibration period). Surface tension measurements of each solution considered were repeated until consistent values were obtained for three consecutive measurements (<0.1 mN/m variation at 25 ± 1 °C). These three measurements were then averaged to yield the surface tension of the solution reported here.

Determination of the Amount of SRB Unbound to SDS Micelles. In order to determine the amount of SRB incorporated into SDS micelles, aqueous solutions of 9 mM SRB were prepared, with varying concentrations of SDS (0−64 mM). Five milliliters of each solution was then added to 10 000 molecular weight (MW) filter centrifugation tubes (Sartorius Stedim Biotech, Goettingen, Germany) and subsequently centrifuged at 900*g* for 2 min. Since the aggregation number of an SDS micelle is ∼50 and SDS has a MW of 288.4 g/mol,[42−44] the MW of an SDS micelle is greater than the MW threshold for the selected filter membrane. Assuming that any formed SRB/SDS micelles have an aggregation number comparable to, or larger than, that of an SDS micelle, SRB is expected to be present in the filtrate in only its unbound form (i.e., in monomeric or dimeric form). Note that the rotational speed and duration of centrifugation were chosen such that less than 10% of the solution would pass through the filter (0.2−0.4 mL). This limits the extent of micelle disassociation in the retentate, which is similar to previously reported protocols used to separate monomers from self-assembled aggregates.[45] A 20 μL volume of the permeate was then diluted to 20 mL (1000-fold dilution), to ensure that the SRB molecules being assayed were in monomeric form. The concentration of SRB was then quantified using a UV/vis spectrophotometer (DU800, Beckman Coulter Inc., Brea, CA) at a wavelength of 560 nm (the observed peak absorbance of SRB). For each SDS concentration considered, the amount of unbound SRB was then reported as the ratio of the concentration of SRB in the filtrate divided by the initial amount of SRB in solution (9 mM).

Testing the Ability of SRB To Enhance Skin Permeability. Previously published protocols[46,47] were utilized for the storage and preparation of skin samples. Skin samples utilized in the study were harvested from the back and flank of Yorkshire pigs in accordance with the MIT Committee on Animal Care. Skin electrical resistivity, *R*, is known to scale directly with skin permeability, and provides an accurate, instantaneous measure of the structural state of the skin.[48] Previously published methods[46−49] were followed to measure *R* of each skin sample. Pretreatment of skin samples by low-frequency ultrasound was also carried out according to previously published methods,[46,47] at an intensity of 7.5 W/cm^2, duty cycle of 50% (5 s on, 5 s off), and tip displacement of 3 mm for 10 min of ON time (replacing the coupling medium every 2 min to minimize thermal effects). Interested readers should refer to refs 46−49 for complete experimental details.

Molecular Dynamics Simulations. To simulate the adsorption of a single SRB molecule at the air/water interface, an SRB molecule was initially positioned at the center of a water box. The size of the water box was chosen to be sufficiently large ($4 \times 4 \times 10$ nm^3) such that the concentration of SRB in water (10.4 mM) corresponds to less than 1/2 its experimental solubility. The water box was sandwiched between two large layers of vacuum ($4 \times 4 \times 5$ nm^3 each) in order to mimic the air/water interfaces. Note that, in all the simulations reported here, sodium counterions were added by replacing the corresponding number of water molecules to maintain electroneutrality of the simulated systems. As the simulation proceeded, the SRB molecule gradually diffused and eventually adsorbed at the air/water interface after 25 ns. The simulation was run for an additional 15 ns for data collection. For simulations testing the adsorption of SRB dimers

at the air/water interface, SRB molecules were initially placed randomly at the interface. Simulations were then run in a fashion identical with that for the single SRB monomer case described above. After equilibration, both SRB monomers and dimers were observed in the bulk solution and adsorbed at the interface. To determine the dimer hydration data, the longest adsorbed stable SRB dimer was selected and tracked for 4 ns for the data analysis.

Following the procedure introduced by Stephenson et al., the relative hydration of each atomic group in SRB was defined as the ratio between the number of water contacts around each atomic group computed in the SRB adsorption simulation, relative to the number of water contacts computed in the SRB monomer simulation.[50] Note that the SRB monomer simulation was carried out by solvating and equilibrating a single SRB molecule in a water box for 5 ns.

To simulate the aggregation of SRB molecules in the bulk water phase, the SRB molecules were positioned randomly in the simulation box, followed by solvating them with randomized water molecules. Five different SRB concentrations were considered, corresponding to 6−49 SRB molecules in the simulation box. Each simulation was equilibrated for 30 ns with the last 10 ns used for data analysis. During the bulk simulations, the formation of SRB dimers was observed and dominated the population of SRB aggregates (with few monomers and trimers observed). In order to better understand the orientation between SRB molecules that form dimers, the angular distribution function of the angle between the pendant groups of SRB molecules in the dimeric state was computed for the lowest SRB concentration case.

To simulate the interactions between the SRB and SDS molecules, 10 SRB and 40 SDS molecules were positioned randomly in the simulation box, followed by solvating them with randomized water molecules. Note that the total number of SRB and SDS molecules was selected to be similar to the aggregation number of an SDS micelle (∼50). A second simulation was also conducted, keeping the concentration of SDS and SRB constant, but with 30 SRB and 120 SDS molecules in the simulation box. The larger simulation was conducted to check our hydration calculations, because it is known that the amount of free monomer present can affect the micelle aggregation number due to the long time scales associated with micellar fission.[51] The simulations were equilibrated for 60 ns, with the last 30 ns used for data analysis. Two SRB−SDS micelles were formed during the 50 molecule simulation and eventually stabilized, with ∼6 micelles forming in the larger simulation. Relative hydration calculations for both simulations were carried out, and the values obtained were found to be nearly identical. The relative hydration diagram reported in the text corresponds to that of the larger micelle in the 50 molecule simulation. Note that the relative hydrations of the SRB and SDS molecules in this case were defined as the number of water contacts around each atomic group in the micellar state relative to the hydration of that atomic group in a bulk aqueous monomer simulation.[50] The SDS monomer simulation was conducted as discussed earlier for the SRB case.

Water molecules were modeled using the standard SPC/E model,[52] with bond lengths constrained using the SETTLE algorithm.[53] SRB and SDS molecules were modeled using the OPLS-AA force field.[54] Previously published force-field parameters were utilized for SDS and rhodamine dyes.[55,56] The +1 charge on the xanthene structure was delocalized symmetrically over the xanthene rings, as in previously published studies[55] (note that the depiction of a localized +1 charge in Figure 1 is for illustrative purposes only). Bond lengths in the SRB and SDS molecules were constrained using the parallel version of the LINCS algorithm.[57,58] van der Waals (vdW) attractions and hard-core steric repulsions were treated with a cutoff distance of 0.9 nm, which falls within the typical range of cutoff values used in other studies.[59,60] The vdW attractions and the hard-core steric repulsions between different atoms were calculated from the Lennard-Jones potential using the standard geometric averaging rule which is implemented in the OPLS-AA force field.[54] Long-range electrostatic interactions were treated using the particle mesh Ewald (PME) summation method.[61,62] The equations of motion were integrated with a time step of 2 fs using the Verlet (leapfrog) algorithm.[63,64] SRB adsorption at the air/water interface was simulated under the *NVT* ensemble (constant number of atoms, constant volume, and constant temperature of 298.15 K), while all other simulations were conducted under the *NPT* ensemble (constant pressure of 1 bar instead of constant volume) in order to best mimic the experimental conditions. The velocity-rescaled Berendsen thermostat was implemented to maintain a constant temperature in the simulated system.[65] The pressure was coupled to an isotropic Berendsen barostat.[66] Periodic boundary conditions were applied in all three directions. The trajectories corresponding to all the atoms in the system were saved every 10 000 steps (20 ps) to satisfy the ergodicity criterion for data analysis.[67] All the simulations presented here were carried out using the GROMACS 4.0 software package.[68]

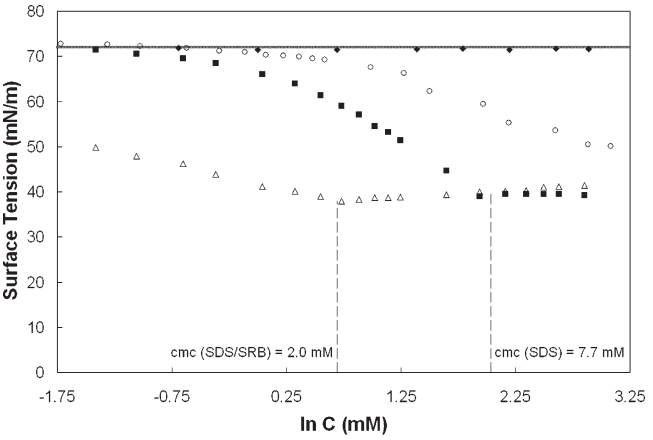

Figure 2. Surface tension versus concentration data for aqueous solutions of allura red (◆), SRB (○), SDS (■), and SDS with 9 mM SRB (△). The vertical dashed lines denote the cmc's of the specified solutions. The horizontal gray bar represents the measured surface tension of pure water.

RESULTS AND DISCUSSION

Adsorption of SRB at the Air/Water Interface. The surface tension measurements revealed that SRB adsorbs at the air/water interface, as reflected in the observed concentration-dependent reduction in the surface tension of aqueous SRB solutions (see Figure 2, open circles). This behavior is in stark contrast to the effect of allura red (red food coloring), where no decrease in surface tension is observed as a function of concentration with this nonamphiphilic dye (see Figure 2, filled diamonds). At the highest SRB concentration considered (22 mM), the surface tension reduction was found to be ∼23 mN/m, which is quite significant considering that SDS was found to decrease the

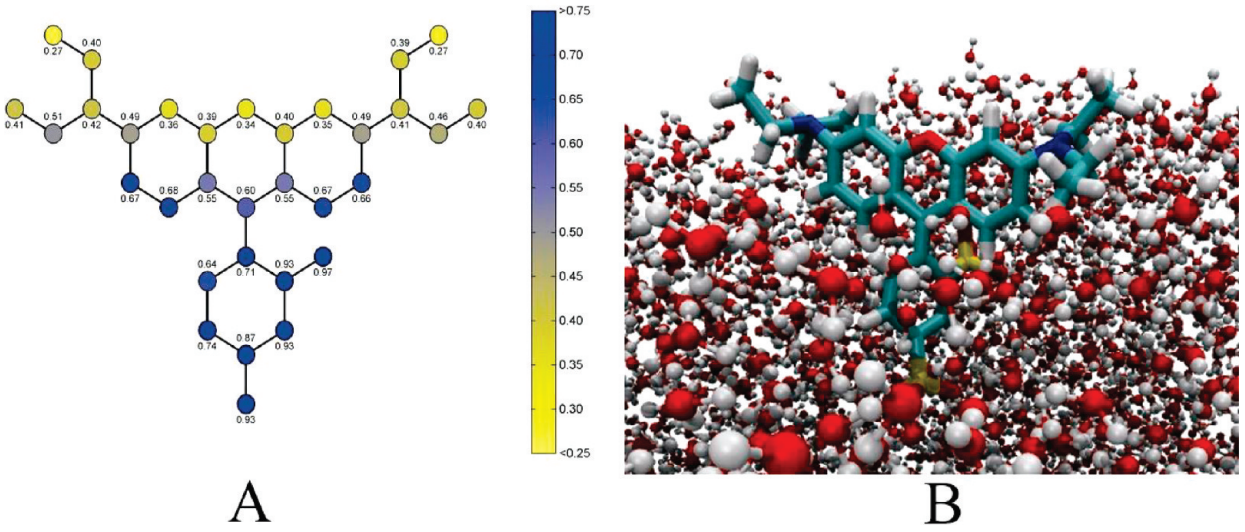

Figure 3. (A) Relative hydration of an SRB molecule adsorbed at the air/water interface. The blue color corresponds to a group with hydration similar to that in bulk aqueous solution, while the transition to yellow corresponds to groups in less hydrated states. The number adjacent to each atomic group denotes the relative hydration. (B) Equilibrium MD simulation snapshot showing an SRB molecule adsorbed at the air/water interface. Color legend: yellow, sulfur; red, oxygen; white, hydrogen; blue-green, carbon; and dark blue, nitrogen.

surface tension of water by ~33 mN/m above its cmc. The surface excess of SRB was calculated from the Gibbs adsorption equation,[69] assuming complete dissociation of sodium ions from the sulfonate groups, in the linear region of the data (2−22 mM) and was found to be 1.18×10^{-6} mol/m^2, which corresponds to 140 Å^2/molecule. As a point of comparison, the surface excess of SDS was found to be 3.56×10^{-6} mol/m^2, in the linear region below the cmc (3−7 mM, Figure 2, squares), which corresponds to 46.6 Å^2/molecule, a value that is consistent with previously reported values (for example, 46 Å^2/molecule at 4 mM[70]). The higher surface excess of SDS, relative to that of SRB, reflects the fact that more SDS molecules can adsorb at the interface, per unit area, than SRB molecules. In view of the chemical structures of SRB and SDS shown in Figure 1, this result is expected because SRB is generally bulkier than SDS.

MD simulations of SRB molecules near the air/water interface were carried out to elucidate the adsorption behavior of SRB. The final state of the simulation, with a single SRB molecule adsorbed at a clean air/water interface, is shown in Figure 3B. Figure 3A shows the relative hydration of different atomic groups in the SRB molecule when adsorbed at the air/water interface, relative to the fully hydrated state in bulk aqueous solution (note that the atomic groups in Figure 3A correspond to the SRB structure shown in Figure 1). In addition, note that in the simulations, the pendant group and the three-ring xanthene structure actually lie out of plane from each other, contrary to the two-dimensional representation used in the figures for clarity. As expected, the simulation revealed that the pendant group of SRB, which contains the two charged sulfonate atomic groups, resides within the bulk aqueous phase. Conversely, a clear division is observed in the xanthene structure, with the carbon groups located closest to the pendant group remaining significantly hydrated (as reflected in the relative hydration of these groups being greater than 0.6), with the rest of the SRB molecule in various states of dehydration (relative hydrations less than 0.6), indicating that these groups are located, on average, in the air phase. It has been previously shown, in similar investigations regarding the relative hydration of amphiphilic molecules in micelles, that relative hydration values greater than 0.6 correspond to the hydrophilic domain of the surfactant molecule (the "head"), while hydration values below 0.6 correspond to the hydrophobic region of the surfactant molecule (the "tail").[71] Therefore, extending this criterion to a molecule adsorbed at an interface, a clear division between head and tail regions of SRB can be made by laterally bisecting the xanthene structure, with the section of SRB containing the pendant group comprising the head of the surfactant. The combined experimental and simulation data conclusively demonstrate that SRB is indeed an amphiphile and preferentially adsorbs at the air/water interface.

Note that no cmc is observed for SRB in aqueous solution (open circles in Figure 2), because a solubility limit is observed before a plateau is reached in the surface tension versus concentration curve. This should be contrasted with the behavior of SDS in aqueous solution, which exhibits a clear plateau in surface tension at its cmc (7.67 mM; see the squares in Figure 2). MD simulations were carried out at various SRB concentrations in bulk aqueous solution to elucidate this finding. The simulations revealed primarily dimer formation at all SRB concentrations tested, with very few trimers, and no higher-order SRB aggregates were observed, thus confirming the inability of SRB to form conventional micelles by itself. The ability of SRB to form dimers in aqueous solution has previously been shown experimentally.[20] At the higher SRB concentrations simulated, most of the SRB molecules formed dimers, with few SRB monomers observed. The dimers (see Figure 4A) were found to lie approximately parallel to each other in the plane of the xanthene rings, where the most likely angle between the plane of the pendant groups of each SRB molecule was found to be 75° (for a definition of α, see Figure 4A). The angular distribution function of the angle between the pendant groups, α, of the two SRB molecules forming the dimer is shown in Figure 4B.

In MD simulations carried out at higher SRB surface concentrations, dimers were observed to form at the air/water interface, as shown in Figure 5B, along with adsorbed SRB monomers. SRB molecules were found to interchange between monomeric and dimeric states during the time scale of the simulation, although

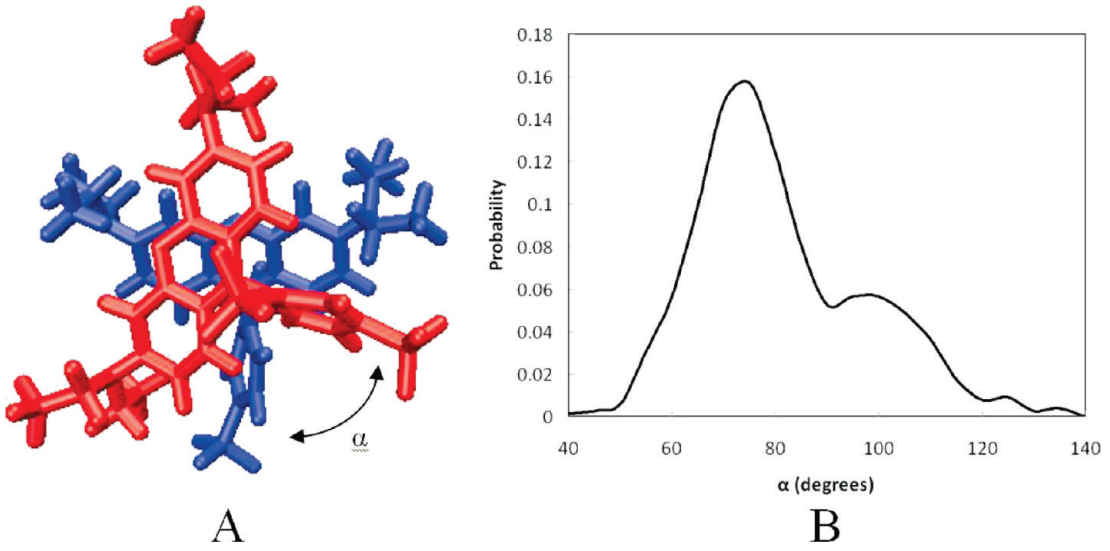

Figure 4. (A) MD simulation snapshot of the orientation of an SRB dimer in bulk aqueous solution, where α is the angle between the planes of the pendant groups of each SRB molecule in the dimer (each SRB molecule is shown in a different color for clarity). (B) Angular distribution function of α.

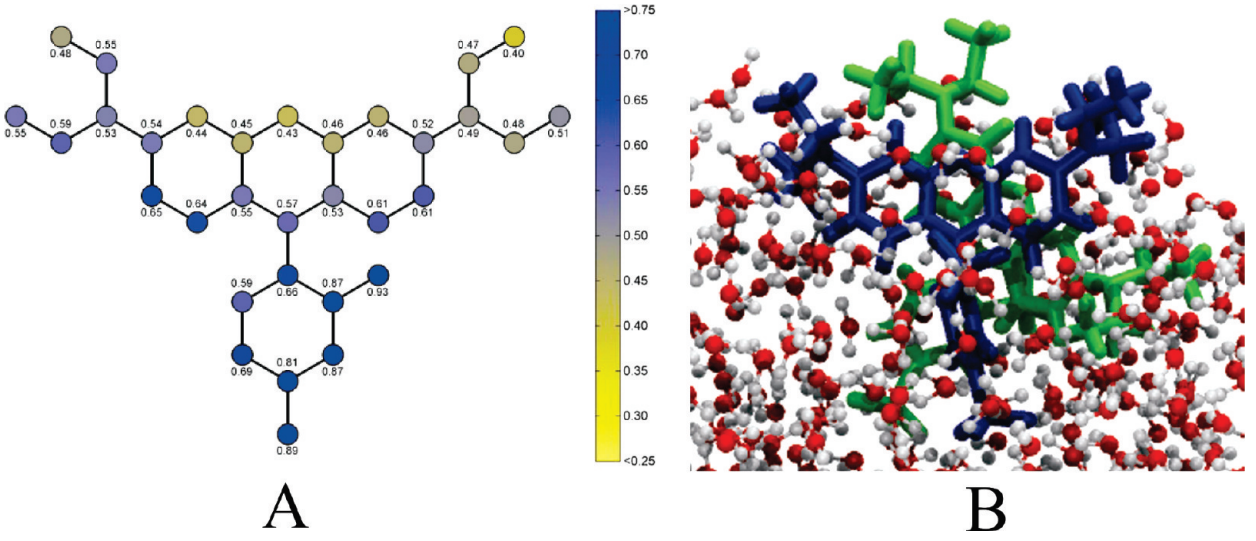

Figure 5. (A) Relative hydration of an SRB molecule adsorbed at the air/water interface in the dimer state. The blue color corresponds to groups with hydration similar to that in bulk aqueous solution, while the transition to yellow color corresponds to groups in less hydrated states. The number adjacent to each atomic group denotes the relative hydration. (B) Equilibrium MD simulation snapshot of SRB adsorbed at the air/water interface in the dimer state. The two SRB molecules of the adsorbed dimer are shown in different colors for clarity.

some stable adsorbed dimers were observed to exist for large durations of the simulation (>4 ns). The relative hydration of SRB in a stable adsorbed dimer (see Figure 5A) was distinctly different than that in the adsorbed monomer state (see Figure 3A). Specifically, it was observed that one of the SRB molecules in the adsorbed dimer was oriented approximately parallel to the air/water interface (see Figure 5B), as in the case of an adsorbed monomer, while the other molecule was offset by approximately 75°, as expected from the angular distribution function in Figure 4B. However, due to the fact that the offset SRB molecule in the dimer extends upward into the air phase, the SRB molecule parallel to the surface of the air/water interface was forced slightly deeper into the water phase than in the case of an adsorbed SRB monomer. When averaged over both SRB molecules in the dimer (each SRB molecule may alternatively be found parallel to the air/water interface during the simulation, as the dimer rotates), greater hydration of the SRB molecule was observed in the adsorbed dimer state than in the adsorbed monomer state, which is clearly seen by comparing Figures 5A and 3A. In spite of the difference in hydration states, the same qualitative relative hydration profile trends are seen between adsorbed SRB monomers and dimers, with much greater hydration of the sulfonate-containing pendant group and decreased hydration in groups further from the pendant group. However, because the adsorbed SRB monomer can extend further into the air phase, compared to the average configuration of an SRB molecule adsorbed at the interface as a dimer, there is greater dehydration of the groups furthest from the pendant group for the monomer case relative to the dimer case.

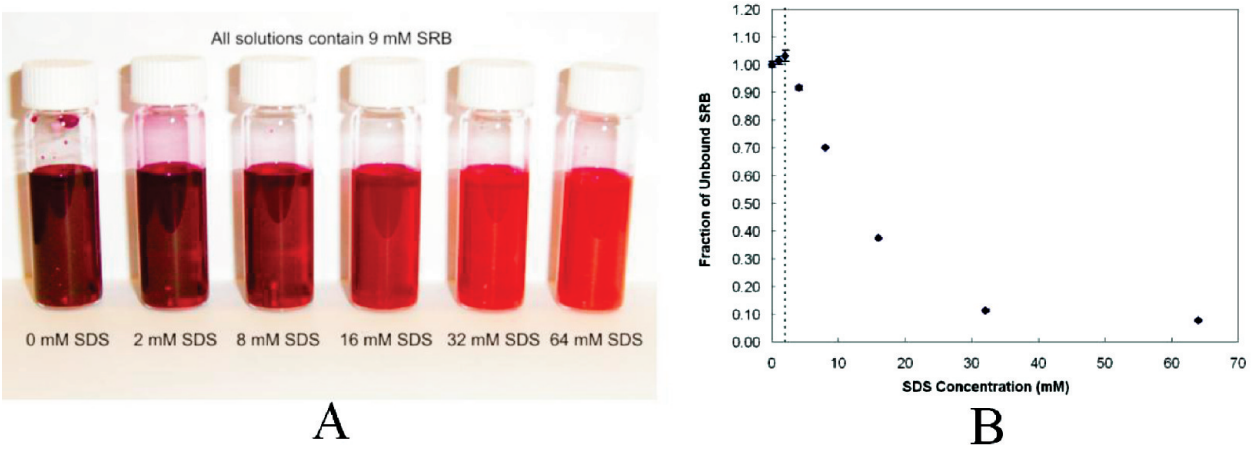

Figure 6. (A) Color change in 9 mM aqueous solutions of SRB with increasing SDS concentration. (B) Fraction of SRB molecules that are not incorporated into SDS micelles, relative to the total concentration of SRB in solution, as a function of SDS concentration. The vertical dashed line corresponds to the cmc of SDS in a 9 mM SRB solution (2.0 mM), and the error bars correspond to a 95% confidence interval on the data.

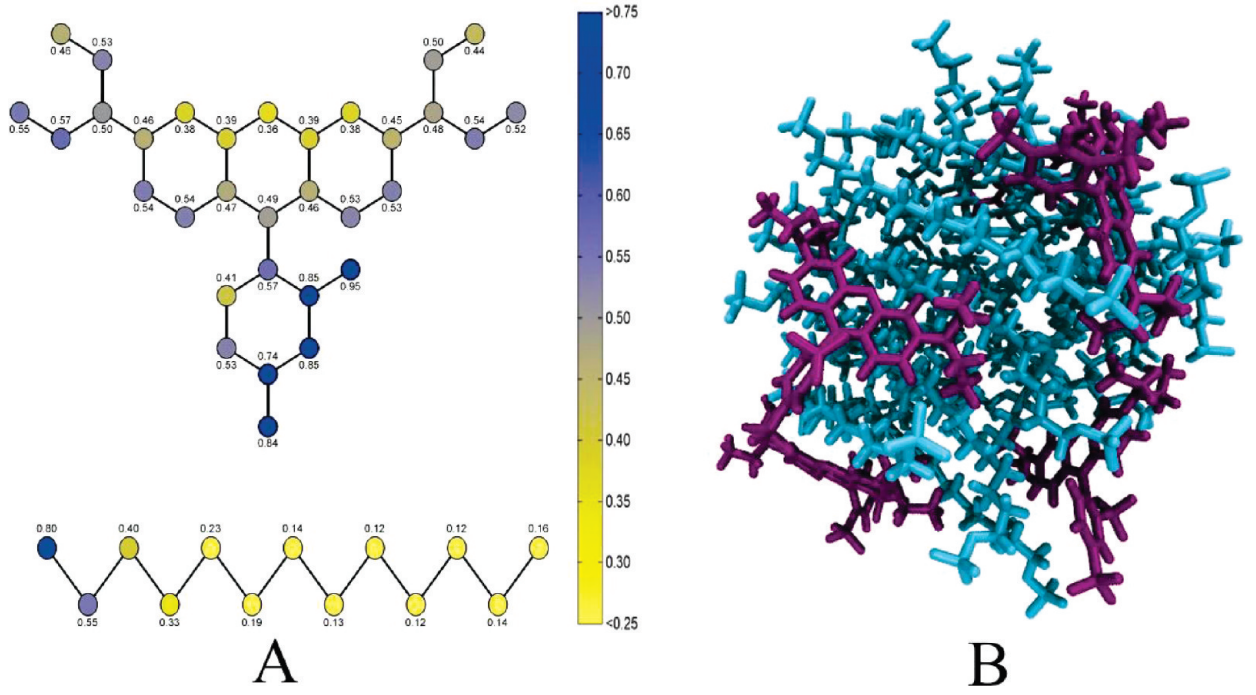

Figure 7. (A) Relative hydration of an SRB molecule solubilized in an SDS micelle. The blue color corresponds to groups with hydration similar to that in bulk aqueous solution, while the transition to yellow color corresponds to groups in less hydrated states. The number adjacent to each atomic group denotes the relative hydration. (B) Equilibrium MD simulation snapshot of SRB incorporated into an SDS micelle. Blue corresponds to SDS molecules, while purple corresponds to SRB molecules.

Interaction of SRB with SDS in Aqueous Solution. The absorption and emission of fluorescent dyes can be strongly affected by their interactions with surfactants. Figure 6A clearly shows how the visible color and opacity of a 9 mM SRB aqueous solution changes when the concentration of SDS is varied between 0 and 64 mM. Furthermore, the addition of SRB to aqueous solutions containing SDS was found to decrease the cmc of SDS from a value of 7.67 mM (without SRB), to a value of 2.00 mM (with 9 mM SRB; see Figure 2). As a point of comparison, the cmc of SDS in allura red (which has been shown to be nonamphiphilic; see black diamonds in Figure 2), was tested and found to remain equal to the cmc of SDS (cmc =7.62 mM) at low allura red concentrations (0.5 mM). Note that at higher concentrations of allura red, or any salt, there will be a decrease in the cmc due to electrostatic screening and counterion binding effects. At 9 mM allura red, the cmc of SDS was found to be 4.50 mM, which is still higher than that found for SDS in 9 mM SRB, despite allura red being a 1:2 electrolyte (two additional sodium ions per mole of allura red) and SRB being a 1:1 electrolyte (one additional sodium ion per mole of SRB). Clearly, this shows that the inclusion of the amphiphilic SRB increases the thermodynamic driving force for micellization compared to the nonamphiphilic allura red, as ionic effects alone cannot explain the observed decrease in the cmc. In addition, Figure 6B shows

that SRB is incorporated within SDS micelles, as reflected by a decrease in the fraction of unbound SRB monomers with increasing SDS concentration (the total SRB concentration in each solution is constant at 9 mM). At an SDS concentration which is twice the cmc of SDS in the presence of 9 mM SRB (4 mM SDS), approximately 10% of the SRB molecules are incorporated into SDS micelles. Furthermore, at 16 times the cmc of SDS in the presence of 9 mM SRB (32 mM), nearly 90% of the SRB molecules are incorporated into SDS micelles (see the fraction of unbound SRB in Figure 6B at the specified SDS concentrations). At intermediate SDS concentrations (between 4 and 16 mM SDS), the molar ratio between SDS and SRB in the micelles is about 3:1, with the molar ratio increasing as the concentration of SDS increases thereafter (5:1 at 32 mM and 10:1 at 64 mM). Note that we have used the term "incorporated into SDS micelles" rather than "co-micellized", because the solubility limit of SRB precludes single-component SRB micelle formation in aqueous solution, in spite of the clear amphiphilicity exhibited by SRB.

In order to gain a molecular-level understanding of the experimental observations made, including the incorporation of SRB molecules into SDS micelles, MD simulations were carried out on systems comprising SDS and SRB. In the initial configuration of these simulations, the SRB and SDS molecules were randomly placed and oriented in the simulation box. Self-assembly was observed to occur as the simulation proceeded. An equilibrium snapshot of the final configuration of one of the micelles that formed is shown in Figure 7B. The molar ratio of SDS to SRB in the simulated micelles is approximately 6:1, which is in general agreement with our experimental data at high concentrations of SDS, reported in the previous paragraph. The SRB molecules were found to be incorporated in the palisade layer (head region) of the SRB/SDS micelles. An examination of the average relative hydration of SRB molecules incorporated in SDS micelles (see Figure 7A) reveals that the majority of the atomic groups of the SRB molecule are incorporated in the micelle, with only the sulfonate groups, and adjacent atomic groups, remaining hydrated to a significant extent (relative hydrations of 0.74−0.95). This is in contrast to the adsorption of SRB at the air/water interface (see Figure 3A), where the entire pendant group and a portion of the xanthene structure exhibit high levels of hydration (0.60−0.97). Comparing the hydration levels of SDS and SRB in the micelle state (Figure 7A, where the atomic groups correspond to the structure shown in Figure 1), it is clear that the sulfonate groups of SRB (relative hydration equal to 0.80−0.95) and the sulfate group of SDS (relative hydration equal to 0.80) are located within approximately the same radial shell of the micelle (forming the outer shell of the micelle). Meanwhile, the remainder of the SRB molecule extends into the micelle core (relative hydrations equal to 0.36−0.57), in the same radial shell where carbons 1−3 of the SDS molecules reside (relative hydrations equal to 0.33−0.55; see Figure 1 for the carbon labeling of SDS). In our simulations, the xanthene structure of the SRB molecule was not found to extend deeply into the micelle core. This is due to (i) packing considerations, which include the large, rigid planar configuration of the xanthene structure relative to the more flexible configuration of the SDS tail, and (ii) electrostatic considerations, which involve the net +1 charge partially distributed across the xanthene structure. Moreover, no SRB dimers were observed in the simulations when SDS micelles were present. SRB absorbance is known to red shift in the monomeric state, compared to the dimer state (spectral data for SRB in the monomer and dimer states can be found in ref 20). Therefore, this finding can explain the observed color shift in the aqueous SRB solutions with increasing SDS concentration (see Figure 6A).

Table 1. Steady-State Enhancement Ratio of Skin Samples Treated with the Specified Coupling Medium and Low-Frequency Ultrasound (20 kHz, 7.5 W/cm^2, 10 min)

coupling medium[a]	n	ER[b]
water	10	1.71 ± 0.67
9 mM allura red	10	1.87 ± 0.62
9 mM SRB	11	54.0 ± 19.6
9 mM SDS	11	79.6 ± 27.1

[a] All solutions are aqueous, containing only the specified components. [b] Errors correspond to a 95% confidence interval on the data.

Case Study: Implications of the Amphiphilic Nature of SRB on Ultrasound-Mediated Transdermal Drug Delivery. Many chemical skin penetration enhancers, particularly amphiphiles, are known to induce synergistic enhancement in skin permeability when combined with low-frequency ultrasound.[40,41] Since SRB exhibits amphiphilic character, as demonstrated above, and has been used extensively in transdermal research under the assumption that it behaves as an inert fluorescent probe,[6,8,12,14,16−19,41,49,72−76] the possibility that SRB could act alone as a skin penetration enhancer was investigated. An SRB concentration of 9 mM was utilized, which is a commonly used concentration of SRB in transdermal research.[8,41,49,73−75] To quantify skin permeability enhancement, an enhancement ratio (ER) was calculated, where ER is defined as the ratio of the posttreatment skin resistivity at steady state (18 h post ultrasound treatment) and the initial skin resistivity of that sample (prior to ultrasound treatment). Skin resistivity is known to scale directly with skin permeability.[48,77] The results of these experiments are summarized in Table 1.

Table 1 shows that skin samples treated with water/ultrasound (control) had a statistically similar enhancement ratio (ER = 1.71 ± 0.67) as those treated with an aqueous solution of 9 mM mM allura red/ultrasound (ER = 1.87 ± 0.62, two-sample t test at 95% confidence). However, the ER corresponding to skin samples treated with an aqueous solution of 9 mM SRB/ultrasound was found to be 30-fold greater than the controls (54.0 ± 19.6), which is a statistically significant difference (p value = 0.004; p value must be below 0.05 for there to be a statistically significant difference at 95% confidence). This clearly shows the ability of SRB to act as a skin permeability enhancer when combined with low-frequency ultrasound, thus further demonstrating its amphiphilic nature. For comparison, the ER for 9 mM SDS (a known surfactant and skin penetration enhancer) is also shown in Table 1 (79.6 ± 27.1). Interestingly, the ERs of SRB and SDS are not statistically significantly different, owing to the generally large variance associated with each sample (p value = 0.15), but also confirming that SRB is a statistically significant skin penetration enhancer.

CONCLUSIONS

We have demonstrated that SRB is an amphiphilic molecule that preferentially adsorbs at an air/water interface, bringing about a considerable decrease in the surface tension of pure water (23 mN/m reduction). MD simulations revealed that SRB is thermodynamically stable in its adsorbed state, both as monomers and as dimers, with clearly defined head and tail regions as

quantified by the hydration of its atomic groups, similar to conventional surfactants. Furthermore, SRB was shown to be able to incorporate into SDS micelles, which results in a dramatic decrease in the cmc of SDS. Because of its incorporation into SDS micelles, SRB was observed to have a significant shift in color and opacity in aqueous solution with increasing SDS concentration. MD simulations revealed that the SRB molecules reside mainly in the palisade layer of the SDS micelles. A case study on skin permeability enhancement by ultrasound and SRB showed that SRB acts as a synergistic skin penetration enhancer, much like many traditional surfactants.

The study presented here demonstrates that even highly water-soluble fluorescent dyes can behave as amphiphiles. In many previous studies, SRB has been assumed to be an inert dye and, therefore, was utilized as a simple colorimetric dye or model hydrophilic permeant. However, the present study shows that one must pay careful attention when selecting an appropriate dye, or fluorescent probe, in a given system. SRB can interact strongly with other surfactants, inducing significant changes in bulk and interfacial properties of aqueous solutions. We therefore recommend that if a fluorescent probe is not needed, it is best to choose the simplest possible dye, such as allura red (red food coloring). If, however, a fluorescent dye is required, special care should be taken to ensure that the dye does not interact with other components of the system. The present study also demonstrates that molecular dynamics simulations can be utilized effectively to study the organization and hydration of dyes in bulk solution, at interfaces, and in micellar environments. These types of studies have previously been carried out using more tedious, experimentally intensive spectroscopic methods. However, using the approach presented here, it may be possible to more easily investigate multiple fluorescent dyes in order to aid in the selection of an appropriate dye for a given system.

AUTHOR INFORMATION

Corresponding Author

*Telephone: (617) 253-4594. Fax: (617) 252-1651. E-mail: dblank@mit.edu.

ACKNOWLEDGMENT

B.E.P., D.B., and R.L. acknowledge funding from the National Institutes of Health (Grant EB-00351) and the U.S. Army Research Office through the Institute for Soldier Nanotechnologies at MIT (Grant DAAD-19-02-D-002). S.L., J.D.M., and D.B. acknowledge funding from the DuPont−MIT Alliance. The contents of this paper represent solely the views of the authors and do not necessarily reflect the position of the U.S. Government or other funding source. No official endorsement should be inferred.

REFERENCES

(1) Behrens, H.; Beims, U.; Dieter, H.; Dietze, G.; Eikmann, T.; Grummt, T.; Hanisch, H.; Henseling, H.; Käss, W.; Kerndorff, H. *Hydrogeol. J.* **2001**, *9*, 321.

(2) Kasnavia, T.; De Vu, D. *Ground Water* **1999**, *37*, 376.

(3) Takahashi, N.; Kishimoto, T.; Nemoto, T.; Kadowaki, T.; Kasai, H. *Science* **2002**, *297*, 1349.

(4) Vichai, V.; Kirtikara, K. *Nat. Protoc.* **2006**, *1*, 1112.

(5) Skehan, P.; Storeng, R.; Scudiero, D.; Monks, A.; McMahon, J.; Vistica, D.; Warren, J.; Bokesch, H.; Kenney, S.; Boyd, M. *J. Natl. Cancer Inst.* **1990**, *82*, 1107.

(6) Ghosh, S.; Kim, D.; So, P.; Blankschtein, D. *Int. J. Cosmet. Sci.* **2009**, *31*, 323.

(7) Jiang, J.; Geroski, D.; Edelhauser, H.; Prausnitz, M. *Invest. Ophthamol. Visual Sci.* **2006**, *47*, 3011.

(8) Kushner, J.; Kim, D.; So, P.; Blankschtein, D.; Langer, R. *J. Invest. Dermatol.* **2007**, *127*, 2832.

(9) Lee, J.; Jee, S.; Chan, C.; Lo, W.; Dong, C.; Lin, S. *J. Invest. Dermatol.* **2008**, *128*, 2240.

(10) Lin, Y.; Skaff, H.; Emrick, T.; Dinsmore, A.; Russell, T. *Science* **2003**, *299*, 226.

(11) Saito, R.; Krauze, M.; Noble, C.; Tamas, M.; Drummond, D.; Kirpotin, D.; Berger, M.; Park, J.; Bankiewicz, K. *J. Neurosci. Methods* **2006**, *154*, 225.

(12) Simonsson, C.; Smedh, M.; Jonson, C.; Karlberg, A.-T.; Ericson, M. B. Two photon microscopy for studies of xenobiotics in human skin. In *Biophotonics 2007: Optics in Life Science*; SPIE: Munich, Germany, 2007; Vol. 6633; p 663320.

(13) Takahashi, N.; Nemoto, T.; Kimura, R.; Tachikawa, A.; Miwa, A.; Okado, H.; Miyashita, Y.; Iino, M.; Kadowaki, T.; Kasai, H. *Diabetes* **2002**, *51*, S25.

(14) Yu, B.; Dong, C.; So, P.; Blankschtein, D.; Langer, R. *J. Invest. Dermatol.* **2001**, *117*, 16.

(15) Yu, B.; Dong, C.; So, P.; Blankschtein, D.; Langer, R. Application of two-photon microscopy to elucidate oleic-acid-induced changes in microscale transdermal transport processes. *Proc. SPIE* **2001**, *4262*, 217.

(16) Yu, B.; Kim, K.; So, P.; Blankschtein, D.; Langer, R. *J. Invest. Dermatol.* **2002**, *118*, 1085.

(17) Yu, B.; Kim, K.; So, P.; Blankschtein, D.; Langer, R. *J. Invest. Dermatol.* **2003**, *120*, 448.

(18) Dong, C. Y.; Yu, B.; Kaplan, P. D.; So, P. T. *Microsc. Res. Tech.* **2004**, *63*, 81.

(19) Lin, S.; Lee, J.; Lin, C.; Chan, C.; Lin, M.; Wang, C.; Tsai, T.; Jee, S.; Dong, C. Investigation of the mechanism of transdermal penetration enhancer—a comparison of multiphoton microscopy and electron microscopy. *Proc. SPIE* **2008**, *6842*, 684203.

(20) Chambers, R.; Kajiwara, T.; Kearns, D. *J. Phys. Chem.* **1974**, *78*, 380.

(21) Maiti, N.; Krishna, M.; Britto, P.; Periasamy, N. *J. Phys. Chem. B* **1997**, *101*, 11051.

(22) Tajalli, H.; Ghanadzadeh Gilani, A.; Zakerhamidi, M.; Moghadam, M. *Spectrochim. Acta, Part A* **2009**, *72*, 697.

(23) Uchida, T.; Yamaguchi, A.; Ina, T.; Teramae, N. *J. Phys. Chem. B* **2000**, *104*, 12091.

(24) Osakai, T.; Yamada, H.; Nagatani, H.; Sagara, T. *J. Phys. Chem. C* **2007**, *111*, 9480.

(25) Greef, R.; Frey, J.; Robinson, J.; Danos, L. *Phys. Status Solidi C* **2008**, *5*, 1187.

(26) Kelkar, V.; Valaulikar, B.; Kunjappu, J.; Manohar, C. *Photochem. Photobiol.* **1990**, *52*, 717.

(27) Malik, W.; Chand, P. *J. Electroanal. Chem.* **1972**, *40*, 385.

(28) Bilksi, P.; Chignell, C. *J. Photochem. Photobiol., A* **1994**, *77*, 49.

(29) Bilski, P.; Holt, R.; Chignell, C. *J. Photochem. Photobiol., A* **1997**, *110*, 67.

(30) El-Hachemi, Z.; Mancini, G.; Ribo, J.; Sorrenti, A. *J. Am. Chem. Soc.* **2008**, *130*, 15176.

(31) Maiti, N.; Mazumdar, S.; Periasamy, N. *J. Phys. Chem. B* **1998**, *102*, 1528.

(32) Garcia, M.; Sanz-Medel, A. *Talanta* **1986**, *33*, 255.

(33) Gadelle, F.; Koros, W. J.; Schechter, R. S. *J. Colloid Interface Sci.* **1995**, *170*, 57.

(34) Hachisako, H.; Murakami, R. *Chem. Commun.* **2006**, *2006*, 1073.

(35) Hachisako, H.; Ryu, N.; Murakami, R. *Org. Biomol. Chem.* **2009**, *7*, 2327.

(36) Yu, D.; Zhang, Q.; Wu, C.; Wang, Y.; Peng, L.; Zhang, D.; Li, Z.; Wang, Y. *J. Phys. Chem. B* **2010**, *114*, 8934.

(37) Ferrer, M.; del Monte, F. *Langmuir* **2003**, *19*, 650.

(38) Ray, K.; Badugu, R.; Lakowicz, J. *J. Phys. Chem. C* **2007**, *111*, 7091.

(39) Ray, K.; Nakahara, H. *J. Phys. Chem. B* **2002**, *106*, 92.

(40) Mitragotri, S.; Ray, D.; Farrell, J.; Tang, H.; Yu, B.; Kost, J.; Blankschtein, D.; Langer, R. *J. Pharm. Sci.* **2000**, *89*, 892.

(41) Tezel, A.; Sens, A.; Tuchscherer, J.; Mitragotri, S. *J. Pharm. Sci.* **2002**, *91*, 91.
(42) Bruce, C. D.; Berkowitz, M. L.; Perera, L.; Forbes, M. D. E. *J. Phys. Chem. B* **2002**, *106*, 3788.
(43) Chen, J. M.; Su, T. M.; Mou, C. Y. *J. Phys. Chem.* **1986**, *90*, 2418.
(44) Jönsson, B.; Lindman, B.; Holmberg, K.; Kronberg, B. *Surfactants and polymers in aqueous solution*; John Wiley & Sons: Chichester, U.K., 1998.
(45) James-Smith, M.; Alford, K.; Shah, D. *J. Colloid Interface Sci.* **2007**, *315*, 307.
(46) Polat, B. E.; Figueroa, P. L.; Blankschtein, D.; Langer, R. *J. Pharm. Sci.* **2011**, *100*, 512.
(47) Seto, J. E.; Polat, B. E.; Lopez, R. F. V.; Blankschtein, D.; Langer, R. *J. Controlled Release* **2010**, *145*, 26.
(48) Karande, P.; Jain, A.; Mitragotri, S. *J. Controlled Release* **2006**, *110*, 307.
(49) Kushner, J., IV; Blankschtein, D.; Langer, R. *J. Pharm. Sci.* **2004**, *93*, 2733.
(50) Stephenson, B. C.; Beers, K.; Blankschtein, D. *Langmuir* **2006**, *22*, 1500.
(51) Sammalkorpi, M.; Karttunen, M.; Haataja, M. *J. Phys. Chem. B* **2007**, *111*, 11722.
(52) Berendsen, H. J. C.; Grigera, J. R.; Straatsma, T. P. *J. Phys. Chem.* **1987**, *91*, 6269.
(53) Miyamoto, S.; Kollman, P. A. *J. Comput. Chem.* **1992**, *13*, 952.
(54) Jorgensen, W. L.; Maxwell, D. S.; Tirado-Rives, J. *J. Am. Chem. Soc.* **1996**, *118*, 11225.
(55) Stephenson, B.; Beers, K.; Blankschtein, D. *J. Phys. Chem. B* **2007**, *111*, 1063.
(56) Dare-Doyen, S.; Doizi, D.; Guilbaud, P.; Djedaini-Pilard, F.; Perly, B.; Millie, P. *J. Phys. Chem. B* **2003**, *107*, 13803.
(57) Hess, B. *J. Chem Theory Comput.* **2008**, *4*, 116.
(58) Hess, B.; Bekker, H.; Berendsen, H. J. C.; Fraaije, J. G. E. M. *J. Comput. Chem.* **1997**, *18*, 1463.
(59) Tummala, N.; Striolo, A. *ACS Nano* **2009**, *3*, 595.
(60) Xu, Z.; Yang, X.; Yang, Z. *Nano Lett.* **2010**, *10*, 985.
(61) Darden, T.; York, D.; Pedersen, L. *J. Chem. Phys.* **1993**, *98*, 10089.
(62) Essmann, U.; Perera, L.; Berkowitz, M.; Darden, T.; Lee, H.; Pedersen, L. *J. Chem. Phys.* **1995**, *103*, 8577.
(63) Hockney, R. W.; Goel, S. P.; Eastwood, J. W. *J. Comput. Phys.* **1974**, *14*, 148.
(64) Verlet, L. *Phys. Rev.* **1967**, *159*, 98.
(65) Bussi, G.; Donadio, D.; Parrinello, M. *J. Chem. Phys.* **2007**, *126*, 014101.
(66) Berendsen, H.; Postma, J.; Van Gunsteren, W.; DiNola, A.; Haak, J. *J. Chem. Phys.* **1984**, *81*, 3684.
(67) Leach, A. *Molecular Modelling: Principles and Applications*; Addison-Wesley Longman Ltd.: Upper Saddle River, NJ, 2001.
(68) Hess, B.; Kutzner, C.; van der Spoel, D.; Lindahl, E. *J. Chem. Theory Comput.* **2008**, *4*, 435.
(69) Hiemenz, P.; Rajagopalan, R. Adsorption from Solution and Monolayer Formation. In *Principles of Colloid and Surface Chemistry*, 3rd ed.; Marcel Dekker, Inc.: New York, 1997; p 327.
(70) Purcell, I.; Lu, J.; Thomas, R.; Howe, A.; Penfold, J. *Langmuir* **1998**, *14*, 1637.
(71) Stephenson, B. C.; Goldsipe, A.; Beers, K. J.; Blankschtein, D. *J. Phys. Chem. B* **2007**, *111*, 1045.
(72) Kirjavainen, M.; Urtti, A.; Jääskeläinen, I.; Marjukka Suhonen, T.; Paronen, P.; Valjakka-Koskela, R.; Kiesvaara, J.; Mönkkönen, J. *Biochim. Biophys. Acta, Lipids Lipid Metab.* **1996**, *1304*, 179.
(73) Paliwal, S.; Menon, G. K.; Mitragotri, S. *J. Invest. Dermatol.* **2006**, *126*, 1095.
(74) Tezel, A.; Sens, A.; Mitragotri, S. *Pharm. Res.* **2002**, *19*, 1841.
(75) Tezel, A.; Sens, A.; Tuchscherer, J.; Mitragotri, S. *Pharm. Res.* **2001**, *18*, 1694.
(76) Yu, B.; Kim, K.; So, P.; Blankschtein, D.; Langer, R. *J. Pharm. Sci.* **2003**, *92*, 2354.
(77) Bos, J.; Meinardi, M. *Exp. Dermatol.* **2000**, *9*, 165.